JOURNAL OF Materials CHEMISTRY

# X-Ray absorption spectroscopic study on $LaPdO_3$

**Seung-Joo Kim,[a] Sylvain Lemaux,[a] Gérard Demazeau,*[a] Jong-Young Kim[b] and Jin-Ho Choy[b]**

[a]*Institut de Chimie de la Matière Condensée de Bordeaux, UPR CNRS 9048, 87 Avenue A. Schweitzer, 33608 Pessac Cedex, France. Tel: 33-(0)5-56-84-83-58; Fax: 33-(0)5-56-84-27-10; E-mail: demazeau@icmcb.u-bordeaux.fr*
[b]*National Nanohybrid Materials Laboratory, School of Chemistry and Molecular Engineering, Seoul National University, Seoul 151-747, Korea*

***Received 26th July 2001, Accepted 11th January 2002***
***First published as an Advance Article on the web 7th February 2002***

Pd L-edge XANES and Pd K-edge XANES/EXAFS have been studied to investigate the electronic configuration and local structure of Pd in a new perovskite $LaPdO_3$, which was prepared under high pressure. A white line in the Pd L-edge XANES for $LaPdO_3$ is positioned just in the middle of those for divalent ($Pd^{II}O$) and tetravalent ($Zn_2Pd^{IV}O_4$) palladates. The peak intensity for $LaPdO_3$ is also in-between those for PdO and $Zn_2PdO_4$. Pd K-edge XANES spectra for PdO is characterized by a shoulder in the threshold edge due to the planar square coordination of Pd. The absence of such a shoulder in Pd K-edge XANES spectra for $LaPdO_3$ and $Zn_2Pd^{IV}O_4$ suggests a nearly regular octahedral symmetry of ($PdO_6$) in both structures. These XANES results underline that the palladium ions with an oxidation state of III are stabilized with the electronic configuration, $t_{2g}^6\sigma^{*1}$ in $LaPdO_3$. The Pd K-edge EXAFS analysis confirms that ($PdO_6$) octahedra in $LaPdO_3$ are nearly isotropic and the average $Pd^{III}$–O bond distance is $2.06_4$ Å, which is compatible with the average $Pd^{III}$–F bond distance (2.00 Å) estimated from a recent EXAFS study on trivalent palladium fluoride.

## Introduction

Trivalent palladium ion, $Pd^{III}$, has been investigated mainly in fluorides. In early neutron diffraction studies, $PdF_3$ has been characterized as being of the $LiSbF_6$ type structure with a cationic ordering, corresponding to $Pd^{II}Pd^{IV}F_6$.[1] Under high pressure $Pd_2F_6$ has shown a pronounced decrease in resistivity, which suggests the charge redistribution ($Pd^{II} + Pd^{IV} \rightarrow 2Pd^{III}$).[2] $Pd^{III}$ has been stabilized in $NaPdF_4$ using high pressures (7 GPa) and in $K_2NaPdF_6$ at normal pressure.[3,4] EPR spectra for both fluorides revealed $Pd^{III}$ to have a low spin configuration ($t_{2g}^6d_{z^2}^1$) associated with a strong Jahn–Teller effect. In oxide systems, however, trivalent palladium is seldom reported. Only mixed valent palladium (+2.5) has been reported in the series of $APd_2O_4$ (A = rare earth) where the Pd is coordinated by four oxygen atoms forming an approximately square planar ($PdO_4$) group.[5–7] The main obstacle to be overcome in stabilizing the trivalent palladium ion in an oxide lattice is a configurational instability of $Pd^{III}$ ($d^7$) leading to disproportionation into $Pd^{II}$ and $Pd^{IV}$. The tendency to disproportionate becomes more important as the crystal field increases. The stable domain for $Pd^{III}$ in oxide is consequently expected to be very narrow due to the relatively strong field of oxygen ligands.

Recently we made an attempt to solve such a problem and successfully prepared, under high pressure, a new perovskite containing $Pd^{III}$, $LaPdO_3$.[8] The following two facts may be most important for the preparation of this compound: (i) the selection of perovskite structure that is very stable under high pressure, and (ii) the relatively small octahedral tilting in the perovskite structure due to the largest rare-earth ion (La) being in the A-site, which contributes to the formation of a metallic configuration $t_{2g}^6\sigma^{*1}$. It should be noted that for smaller A cations (Gd–Lu, In, and Sc) tetravalent palladates, $A_2Pd_2O_7$ with a pyrochlore structure were obtained[9] under high-pressure conditions similar to those used for $LaPdO_3$.

As often shown in transition metals containing perovskite with degenerated electron configuration, the local structure of transition metals plays a crucial role in determining their physical properties.[10] For example, the cooperative Jahn–Teller effect is observed in the antiferromagnetic insulator $LaMnO_3$. Partial charge disproportionations are found in $CaFeO_3$ and $ANiO_3$ (A = small rare-earth) but not in either $SrFeO_3$ or $ANiO_3$ (A = large rare-earth). For the investigation of such small variations in the electronic structure and the local structure of transition ions, X-ray absorption spectroscopy (XAS) would be one of the most powerful tools. Among the various absorption edges, $L_3$-edge XANES spectra are of particular usefulness since they exhibit prominent features due to a transition from the $2p_{3/2}$ level to unoccupied *n*d states, which are involved in oxidation state changes. EXAFS analysis is also complementary to X-ray diffraction studies because the latter may induce an uncertainty in the determination of the space group and oxygen atomic coordinates in compounds involving a charge disproportionation or a Jahn–Teller distortion.

In the present work, XAS measurements were undertaken at Pd K-edge and Pd $L_3$-edges for $LaPdO_3$. Through a comparison of the XANES spectra of $LaPdO_3$ with those of divalent and tetravalent palladates, we examined the oxidation state and local structure of Pd in $LaPdO_3$. We also carried out EXAFS analysis to determine the Pd–O bond distances.

## Experimental

### Sample preparation and characterization

A polycrystalline $LaPdO_3$ sample was prepared from oxidation of a $La_2Pd_2O_5$ precursor with an oxidizing reagent, $KClO_3$, under high pressure–high temperature (HP-HT) conditions. The mixture of $La_2Pd_2O_5$ and $KClO_3$ with a molar ratio of 1 : 1 was encapsulated in a platinum tube with a diameter of 3 mm. The capsule was separated by NaCl powder from a graphite tube (internal heater) before being heated at 1100–1150 °C under 5 GPa for 10 min. The oxygen content was determined to be $2.98 \pm 0.02$ by redox titration. The detailed procedures for

the preparation and some of the characterizations are described in a previous report.[8]

The X-ray powder diffraction data for $LaPdO_3$ were collected every 0.02° for $3° < 2\theta < 120°$ on a Phillips PW 1050 diffractometer with a monochromator for Cu $K_\alpha$ radiation. The structural parameters were refined using the Rietweld analysis program, FULLPROF.[11] The background level was optimized with a polynomial function and the peak shape was fitted to a pseudo-Vöigt function.

The magnetic susceptibility was measured with SQUID (Quantum Design MPMS-5S) under $H = 1$ T in the 5–300 K temperature range.

As reference samples for the comparison of the XANES spectra, $Pd^{II}O$ (Alrich 99.9+%) and $Zn_2Pd^{IV}O_4$ were selected. $Zn_2PdO_4$ was prepared as indicated in a previous report.[12]

### XANES and EXAFS measurement and data analysis

The XANES spectra of Pd $L_3$-edge (3173 eV) were measured at room temperature in transmission mode with a 0.2 eV energy step using a Si(111) double-crystal monochromator on the beam line D44 of the DCI storage ring (energy: 1.85 GeV, current: 310 mA) in LURE (Orsay, France). Well-dispersed sample powders in cyclohexane were embedded on porous polycarbonate membranes. The amount of sample was precalculated to obtain an optimum absorption jump[13] ($\Delta\mu_t \approx 1$). Harmonics were rejected with a mirror. The spectra were calibrated for energy with the presence of argon traces in the ionization chamber (Ar K-edge: 3202 eV). The spectra were normalized at 3185 eV. The X-ray absorption measurements on the Pd K-edges were carried out at the beam line 10B of the Photon Factory (energy: 2.5 GeV, current: 360 mA; KEK-PF, Tsukuba, Japan). The data were recorded with a spacing of ~0.3 eV for the XANES region and ~1.5 eV for the EXAFS region in transmission mode at room temperature. A Si(311) monochromator channel-cut monochromator was used.

The data analysis for the Pd K-edge EXAFS was performed by using a standard procedure as follows.[14,15] The inherent background in the data was removed by fitting a polynomial to the pre-edge region, and extrapolating through the entire spectrum, from which it was subtracted. The resulting spectra, $\mu(E)$, were normalized to an edge jump of unity in order to compare the XANES features directly with one another. The absorption spectrum for the isolated atom, $\mu_0(E)$, was approximated by a cubic spline. The EXAFS function, $\chi(E)$, was obtained as $\chi(E) = \{\mu(E) - \mu_0(E)\}/\mu_0(E)$.

Further analysis was performed in $k$ space, where the photoelectron wave vector $k$ is defined as $k = \{(2m/h^2)(E - E_0)\}^{1/2}$, where $m$ is the electron mass and $E_0$ is the threshold energy of photoelectron at $k = 0$. The resulting EXAFS spectra were $k^3$ weighted and Fourier transformed in the range of ~3 Å$^{-1}$ $\leqslant k \leqslant$ ~13 Å$^{-1}$ with a Hanning apodization function. In order to determine the structural parameters of the Pd–O bond, a non-linear least-squares curve fitting procedure was carried out for Fourier transformed $k^3\chi(k)$ of the first shell corresponding to the Pd–O bonding pair in the Fourier transform (FT) by using the EXAFS formula on the basis of the plane wave single-scattering description, which can be expressed as follows:

$$\chi(k) = -S_0^2 \sum_i \frac{N_i}{kR_i^2} F_i(k) \exp\{-2\sigma_i^2 k^2\} \exp\{-2R_i/\lambda(k)\} \times \sin\{2kR_i + \phi_i(k)\}$$

The back scattering amplitude, $F_i(k)$, the total phase shift, $\phi_i(k)$, and the photoelectron mean free path, $\lambda(k)$, were theoretically calculated by the curved wave *ab initio* EXAFS code FEFF 5, where the amplitude reduction factor and the Debye–Waller factor were set equal to unity and zero, respectively. In the course of non-linear least-squares curve fitting between experimental $k^3\chi(k)$ and theoretical one, the structural parameters such as the Pd–O bond distance, $R_i$, the amplitude reduction factor, $S_0^2$, the Debye–Waller factor, $\sigma_i^2$, which represents a mean-square relative displacement, and the threshold energy difference, $\Delta E_0$ were optimized as variables. The coordination number, $N_i$, was set equal to six corresponding to the crystallographic value in the entire course of the fitting procedure.

## Results and discussion

### Charaterizations by powder X-ray diffraction and magnetism

X-Ray patterns for the powder obtained by HP-HT reactions are composed of reflections for perovskite phase, KCl and small impurities. The minor impurities (~3%) were $LaPd_2O_4$ and $La_2O_3$, which may be produced from partial decomposition of $LaPdO_3$ by small amounts of water absorbed on the precursor.

All reflections for $LaPdO_3$ (Fig. 1) have been accounted for with a primitive orthorhombic unit cell (space group = *Pbnm*) with $a = 5.5898(3)$ Å, $b = 5.8502(3)$ Å, and $c = 7.8665(4)$ Å. The observed, calculated and difference patterns from Rietveld refinement are shown in Fig. 1. The final factors of the refinement ($R_{wp} = 16.8\%$, $R_{exp} = 9.3\%$, $R_{Bragg} = 6.1\%$ and $\chi^2 = 3.2$) indicate that our refined structure could be acceptable, although some deviations may still exist, especially those of the light element, oxygen. The refined crystallographic information including some bond distances and angles are listed in Table 1. The La–O distances are clearly split into two sets, eight short and four long bonds, due to the strong orthorhombic distortion of the perovskite lattice. The average distance of the eight short La–O bonds (2.57 Å) is consistent with the value (2.56 Å) deduced from the effective ionic radii of $La^{3+}$ (coordination number, CN = 8) and $O^{2-}$ (CN = 4) reported by Shannon.[16] Three kinds of the Pd–O bond distances [2.087(7) Å, 2.12(2) Å, 2.04(2) Å] are deduced from the X-ray diffraction. A significant Jahn–Teller effect, frequently observed for $e_g$ level degenerated systems such as $Mn^{3+}$ ($t_{2g}^3e_g^1$) containing perovskites, is not detected; *i.e.*, the distortion parameter, $\Delta_d = (1/6)\Sigma_{n=1,6}[(d_n - <d>)/<d>]^2$ of the $PdO_6$ octahedron ($\Delta_d = 2.5 \times 10^{-4}$) is much smaller than that of the $MnO_6$ octahedron ($\Delta_d = 33.1 \times 10^{-4}$) in $LaMnO_3$.[17] Interestingly, $\Delta_d$ of the $PdO_6$ octahedron in $LaPdO_3$ is close to those ($\Delta_d = 1.53 \times 10^{-4} - 1.85 \times 10^{-4}$) observed for $ANiO_3$ (A = small rare-earth, such as Ho, Y, Er and Lu) in the metallic regime ($T > T_{IM}$),[18] which may indicate the existence of a similar vibronic character in both systems. Neutron diffraction may provide impoved structural information to discuss this feature of $LaPdO_3$ but the problem of obtaining enough of the compound remains unsolved for the present due to the extreme conditions for preparation.

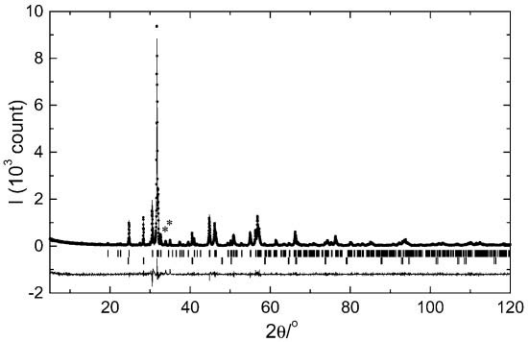


**Fig. 1** Rietveld refinement of $LaPdO_3$ at room temperature. The filled circles represent the experimental data, and the solid line is the calculated profile. The difference is plotted at the bottom of the figure. The upper and and lower ticks indicate the Bragg positions of $LaPdO_3$ and KCl, respectively. The * marks indicate minor impurities (~3%).

**Table 1** Structural parameters, main bond distances and selected bond angles for $LaPdO_3$

$a = 5.5898(3)$ Å, $b = 5.8502(3)$ Å, $c = 7.8665(4)$ Å, $Z = 4$

| | Site | $G$ | $x$ | $y$ | $z$ | $B$/Å$^2$ |
|---|---|---|---|---|---|---|
| La | 4c | 1 | 0.9864(5) | 0.0595(3) | 0.25 | 0.59(6) |
| Pd | 4b | 1 | 0.5 | 0 | 0 | 0.42(6) |
| O1 | 4c | 1 | 0.120(4) | 0.466(3) | 0.25 | 0.7(3) |
| O2 | 8d | 1 | 0.711(3) | 0.295(2) | 0.044(2) | 0.7(3) |

| | Bond length/Å | | Bond angle/° |
|---|---|---|---|
| La–O1 | 2.27(2) | | |
| La–O1 | 2.50(2) | | |
| La–O1 | 3.43(2) | O1–Pd–O2 | 87.9(9) |
| La–O1 | 3.55(2) | O1–Pd–O2 | 84.2(9) |
| La–O2 (×2) | 2.50(2) | O2–Pd–O2 | 89.4(11) |
| La–O2 (×2) | 2.62(2) | | |
| La–O2 (×2) | 2.77(2) | | |
| La–O2 (×2) | 3.54(2) | Pd–O1–Pd | 141.9(3) |
| $<$La–O$>_{8\ short}$ | 2.57 | Pd–O2–Pd | 153.0(6) |
| $<$La–O$>_{4\ long}$ | 3.52 | | |
| Pd–O1 (×2) | 2.087(7) | | |
| Pd–O2 (×2) | 2.12(2) | | |
| Pd–O2 (×2) | 2.04(2) | | |
| $<$Pd–O$>$ | 2.08 | | |
| $\Delta_d$[a] | $2.5 \times 10^{-4}$ | | |

[a]The distortion parameter $\Delta_d$ of an octahedron $PdO_6$ with an average Pd–O distance $<d>$ is defined as $\Delta_d = (1/6)\Sigma_{n=1,6}[(d_n - <d>)/<d>]^2$. v$d>]^2$. $<d>]^2$.

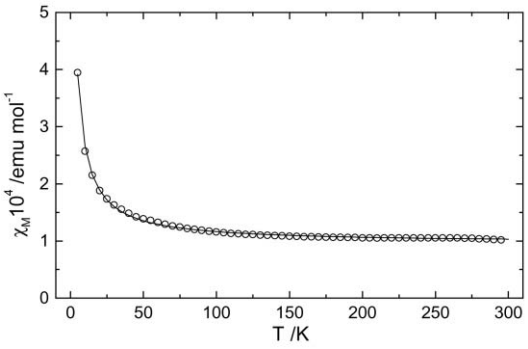


**Fig. 2** Temperature dependence of the molar magnetic susceptibility of $LaPdO_3$ after correction of the core diamagnetic term. The calculated value (solid curve) is obtained from an equation of $\chi = \chi_{pp} - aT^2 + C/T$ with $\chi_{pp} = 1.0 \times 10^{-4}$ emu mol$^{-1}$, $a = 1.1 \times 10^{-10}$ emu (K$^2$ mol)$^{-1}$, and $C = 1.5 \times 10^{-3}$ emu K mol$^{-1}$.

The molar magnetic susceptibility of $LaPdO_3$ is independent of temperature in the range of 60–300 K (Fig. 2). At low temperature (5–60 K) the magnetism is combined with a small Curie component. The temperature independent term after diamagnetic correction corresponds to a Pauli paramagnetic susceptibility, $\chi_{pp}$ ($1.0 \times 10^{-4}$ emu mol$^{-1}$), and suggests that $LaPdO_3$ is metallic.

## Pd $L_3$-edge XANES

The Pd $L_3$-edge XANES spectra (Fig. 3) of the three palladates, PdO, $LaPdO_3$ and $Zn_2PdO_4$ are composed of a main, intense white line (peak a), which primarily corresponds to the electric dipolar transition: $2p_{3/2}{}^6 4d^n \rightarrow 2p_{3/2}{}^5 4d^{n+1}$. In the spectra of PdO and $LaPdO_3$ a second peak (peak b) located at higher energy can be observed. The spectra were analysed by least-squares fit with pseudo-Voigt functions to simulate the form of peaks a and b and an arctangent function was used to simulate the transition to s,d continuum states.[19] The relevant parameters about peak a are listed in Table 2. A linear shift to higher energy of peak a position is clearly observed on going from $Pd^{II}O$ to $Zn_2Pd^{IV}O_4$. The peak position in Pd $L_3$-edge XANES for $LaPdO_3$ is equal to half the energy of those

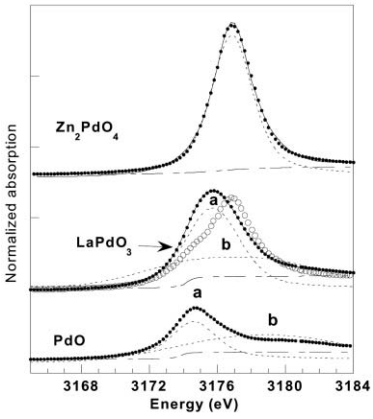


**Fig. 3** Normalized Pd $L_3$-edge spectra for (a) PdO, (b) $LaPdO_3$ and (c) $Zn_2PdO_4$. Solid line: experimental value. Dotted line: pseudo-Voigt contribution. For PdO and $LaPdO_3$ two pseudo-Voigt are necessary, (peak a and peak b). Intensities of the fitted peaks b are enlarged on the figure by a factor of 3. Open circles: average spectra of PdO (50%) and $Zn_2PdO_4$ (50%).

observed in the two other samples. Neither $Pd^{II}$ nor $Pd^{IV}$ are present in $LaPdO_3$ since the spectrum of $LaPdO_3$ does not correspond to the averaged spectrum obtained from 50% of divalent and 50% of tetravalent palladium oxides. Moreover the intensity of the peak (Table 2) in $LaPdO_3$ is also close to the average value of that of $Pd^{II}O$ and $Zn_2Pd^{IV}O_4$. Therefore the oxidation state of Pd in $LaPdO_3$ must be III.

We can compare the present results with a study that was made on the Pd $L_3$ XANES of fluorides for a similar purpose.[20] In the fluoride system it has been shown that, even in the case of

**Table 2** Relevant parameters of the fit of peak **a** obtained from the Pd $L_3$-edge spectra of PdO, $LaPdO_3$ and $Zn_2PdO_4$

| | Intensity | Position/eV | FWHM/eV |
|---|---|---|---|
| $Pd^{II}O$ | 11.3 | 3174.6 | 1.8 |
| $LaPdO_3$ | 26.7 | 3175.7 | 2.2 |
| $Zn_2Pd^{IV}O_4$ | 36.9 | 3176.8 | 1.6 |

the very ionic chemical bond Pd–F, no multiplet effects affect the Pd $L_3$ XANES spectrum, which is probably due to the delocalization of the 4d orbitals. Thus, these effects can also be neglected in more covalent systems as oxides and therefore the peak position and intensity are directly correlated with their oxidation state. Compared with the fluorides, the shift induced by the difference in oxidation state is less prominent in the oxides: it is only 2.2 eV between the $Pd^{II}$ and $Pd^{IV}$ in oxides but 4 eV in fluorides, which is attributed to the lower ionicity of the Pd–O bond as compared with the Pd–F one.

The XANES for PdO exhibits a contribution, peak b, of about 4 eV above the white line. This behaviour must be related to the presence at this energy, in the electronic structure of PdO,[21] of unoccupied states composed of Pd 4d orbitals mixed with O 2p. Such a mixing might also explain the peak b contribution in the spectrum of $LaPdO_3$.

One may notice that peak a in $LaPdO_3$ is broader than the peaks in $Pd^{II}$ and $Pd^{IV}$ oxides (Table 2). Such broadening has been observed in the $L_3$-edges of transition metals in metallic oxides, for example, in $Sr_xLa_{2-x}CuO_4$ by comparing the Cu $L_3$-edge of metallic to insulator cuprates of the same series.[22] The Ni $L_3$-edge of some nickelates also exhibits a broadening due to intrinsic metallic properties.[23] These observations suggest a correlation of this broadening with the metallic state of these oxides.

## Pd K-edge XANES

Normalized Pd K-edge XANES spectra of PdO, $LaPdO_3$ and $Zn_2PdO_4$ are shown in Fig. 4(a). The corresponding second derivative curves are presented in Fig. 4(b) to identify the fine features in the edge region and to locate them more accurately for energy. It is known that K-edge XANES could be affected by the local structure as well as the oxidation states of the absorber.[24] The $Pd^{IV}$ has a regular octahedral symmetry in $Zn_2Pd^{IV}O_4$ with a cubic spinel structure, whereas the $Pd^{II}$ has 4-coordinated square-planar symmetry in PdO. Such different local structures for these compounds may lead to the fact that a shoulder (denoted by A) in the edge threshold ($\sim$24347.5 eV) for PdO is not detected for $Zn_2PdO_4$. Similar shoulders in edge threshold have been observed in K-edge XANES spectra for 3d ions with square-planar or elongated octahedral symmetry. They have been assigned to transitions from 1s levels to π*

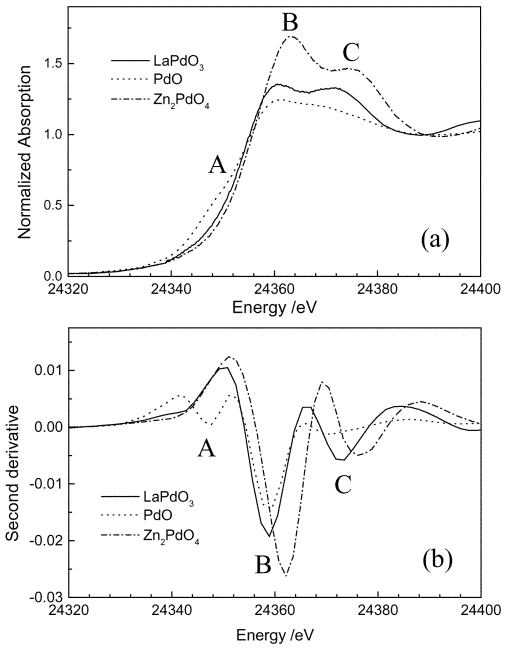


**Fig. 4** (a) Normalized Pd K-edge spectra and (b) their second derivatives for PdO, $LaPdO_3$ and $Zn_2PdO_4$.

non-bonding states in which the $4p_\pi$ orbitals ($5p_\pi$ in the case of $Pd^{II}$) of the metal are involved.[21] The shoulder is also not detected in $LaPdO_3$, from which it can be concluded that $Pd^{III}$ in $LaPdO_3$ has an isotropic octahedral symmetry.

Except for the shoulder in the edge threshold for PdO, two important absorption peaks, B and C, are commonly observed in the three compounds. The peaks B correspond to the transitions to the $\underline{1s}4d^n\ ^1\underline{5p}^1$ final state for $LaPdO_3$ and $Zn_2PdO_4$ and to $\underline{1s}4d^n\ ^1\underline{5p}_\sigma{}^1$ for PdO, respectively. The position of peak B for PdO is nearly same as that for $LaPdO_3$, whereas the for $Zn_2PdO_4$ it shifts to an energy about 3 eV higher than that for $LaPdO_3$. The similarity in position of the B peaks in PdO and $LaPdO_3$ may be only a fortuity due to the different local structures of both the compounds. The energy split between $5p_\sigma$ and $5p_\pi$ is significantly wide in square-planar symmetry for PdO, whereas the energy levels of Pd 5p orbitals in $LaPdO_3$ are degenerated due to its regular octahedral symmetry. The energy levels of the 5p final states for PdO, $LaPdO_3$ and $Zn_2PdO_4$, therefore, could be described as shown in Fig. 5. The nearly same energy of $5p_\sigma$ for $Pd^{II}$ and 5p for $LaPdO_3$ could be the result of a compensation of the following two effects: (i) the energy lowering due to the change of symmetry from planar to octahedral and (ii) the energy rising due to an increase of oxidation state of Pd in $LaPdO_3$. Similar aspects have been observed in Cu K-edge XANES for several copper fluoride compounds[18] with different structures where the absorption edge of octahedral $Cu^{II}$ shifts to lower energy (−1.9 eV) relative to that of square-planar $Cu^{II}$.

The origin of peak C is not clear at present although it also shows a strong dependency on the Pd valence. It may be related to the shake-up process involving Pd 4d → 5p transitions in the core-hole final process and/or multiple scattering.

## Pd K-edge EXAFS

Fig. 6(a) and 6(b) represents the $k^3$ weighted Pd K-edge EXAFS spectra and their Fourier transforms (FT), respectively. The first peak in the FT corresponds to the nearest neighbours of palladium ion, *i.e.*, (Pd–O) shells. In the fitting procedure, only the distance ($R$) and the Debye–Waller factor ($\sigma^2$) were allowed to be refined. However, the coordination number (CN) was fixed to the crystallographic value to be free from the inaccuracies in refining the CN values, since they are strongly correlated with $\sigma^2$. The best fit to the first coordination shell is compared with the experimental spectra in Fig. 6(b) and the fitted structural parameters are listed in Table 3. EXAFS spectra were computed up to $\sim$4.5 Å including multiple scattering terms over third-order (four-legged paths). To extend the fitting procedure to the more distant $R$, it is important to properly treat the single scattering and multiple scattering paths. The most important contributions for 2.0 Å $\leqslant R \leqslant$ 4.5 Å are those from two single scattering (SS), one double scattering (DS) and collinear triple scattering (CTS) paths. The

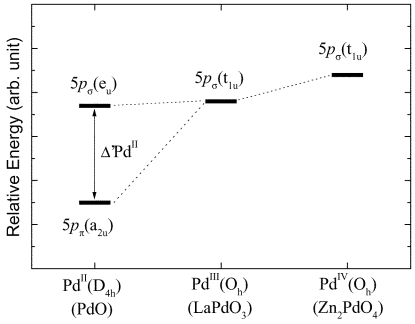


**Fig. 5** Energy level diagram of 5p final states relative to 1s core-hole state for ($Pd^{II}O_4$) plan, ($Pd^{III}O_6$) octahedron and ($Pd^{IV}O_6$) octahedron. In $D_{4h}$ symmetry, the difference between two energy levels corresponds to the final state crystal field splitting ($\Delta$'$Pd^{II}$)

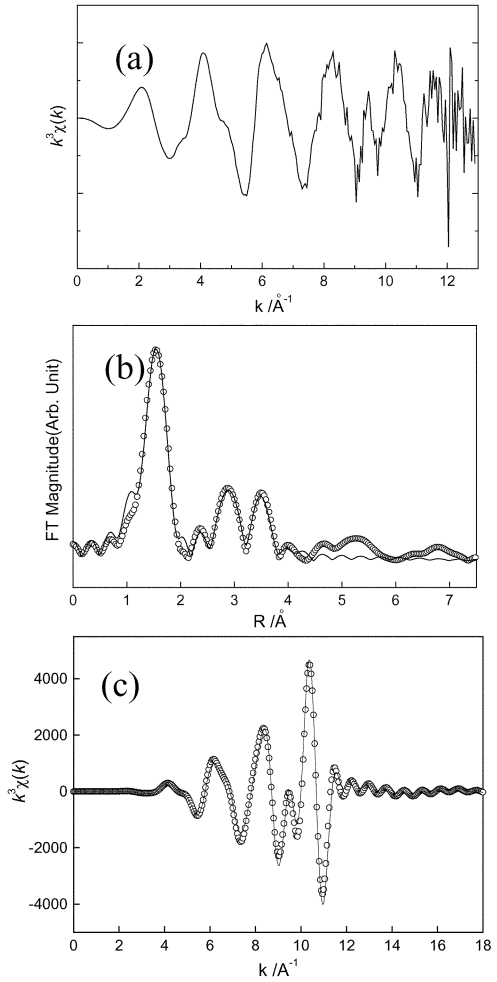


**Fig. 6** (a) The $k^3$-weighted EXAFS spectra, (b) their Fourier transform (open circles) and best fit (solid line) and (c) Fourier-filtered EXAFS spectra (open circles) and best fit (solid line) in the first coordination sphere of the palladium in $LaPdO_3$.

first SS path corresponds to six-coordinated oxygen atoms and the second SS connects the absorber and A-site cations (La). In particular, in the 3–4.5 Å range, CTS (Pd–O–Pd–O–Pd) and DS (Pd–O–Pd–Pd) paths are important as a result of the well-known focusing effect. Other multiple scattering paths are negligible due to both their low multiplicity and non-collinearity.

Fourier-transformed experimental and calculated spectra with multiple scattering paths are compared in Fig. 6(c). The average Pd–O bond distance is calculated at $2.06_4$ Å, which is consistent with XRD results (2.08 Å). Considering the difference ($\Delta r = 0.07$ Å) between the radii of oxide and fluoride ions, the average $Pd^{III}$–O bond distance (2.08 Å) is compatible with the average $Pd^{III}$–F bond distance (2.00 Å) estimated from a recent EXAFS study on $K_2NaPdF_6$ with the elpasolite-type structure where the ($PdF_6$) octahedra exhibit a Jahn–Teller distortion.[20]

It has been evidenced in several systems[25–28] that EXAFS, being sensitive to short-range order, is very suitable for examining whether Jahn–Teller distortion exists or not. For $LaPdO_3$, the Fourier transform of the EXAFS signal displays only one peak for the first oxygen shell and the experimental data are well fitted by nonlinear least-squares calculation based on crystallographic data. This fact suggests that no static Jahn–Teller effects affect the Pd local symmetry in $LaPdO_3$. However, the Debye–Waller factor ($\sigma^2 = 4.4 \times 10^{-3}$ Å$^2$, Table 3) for the Pd–O bond is slightly higher than those for other transition metal–oxygen bonds in several orthorhombic perovskites (for example, the values of $\sigma^2$ are in range of

**Table 3** Pd K-edge EXAFS fitting results for $LaPdO_3$

| Scattering paths[a] | $\Delta E_0$[b]/ eV | $R$[c]/Å, angle/° | Debye–Waller factor/Å$^2$ |
|---|---|---|---|
| 6 × (Pd–O) | −2.47 | 2.064 | 0.0044 |
| 2 × (Pd–La) | −5.50 | 3.24 | 0.0021 |
| 2 × (Pd–La) | −5.50 | 3.38 | 0.0021 |
| 2 × (Pd–La) | −5.50 | 3.50 | 0.0021 |
| 2 × (Pd–La) | −5.50 | 3.82 | 0.0021 |
| 2 × (Pd–Pd) | 1.09 | 3.93 | 0.0031 |
| 4 × (Pd–Pd) | 1.09 | 4.06 | 0.0031 |
| 12 × (Pd–O–Pd–Pd) double scattering | −4.28 | 4.10, 167.4 | 0.0044 |
| 4 × (Pd–O–Pd–O–Pd) collinear triple scattering | 0.48 | 4.06 | 0.0088[d] |
| | 0.48 | 4.17 | 0.0088[d] |
| | 0.48 | 4.24, 180 | 0.0088[d] |

[a]Amplitude factors for all paths are fixed to be the value for Pd–O single scattering. [b]Initial $E_0$ value is 24351.0 eV. [c]The $R$ values, except (Pd–O) single scattering were those of the crystallographic data. [d]It was assumed that the DW factor for CTS (Pd–O–Pd–O–Pd) = 2 × DW factor for SS (Pd–O).[13]

2.9–3.3 × $10^{-3}$ Å$^2$ for $Ru^{IV}$–$O$[29] or $Ir^{IV}$–$O$[15] through similar fitting procedures.), which may indicate some fluctuations in Pd–O bond distances. But the magnitude of the fluctuations is too small to be detected by the present EXAFS analysis.

In addition, the unit-cell parameter ratio, $c/\sqrt{2}a$ (0.995) in $LaPdO_3$ is smaller than 1. The value of $c/\sqrt{2}a$ has been used as a measure for Jahn–Teller effects in perovskite structures. But it should be pointed out that the $c/\sqrt{2}a$ ratio is not the relevant factor for considering some trivalent nickelates ($d^7$), $PrNiO_3$ (0.994) and $NdNiO_3$ (0.999) in order to detect a possible static Jahn–Teller effect.[30] The origin of such anomalous structural features in $Ni^{III}$ and $Pd^{III}$ perovskite should be studied further.

## Conclusions

The Pd L-edge XANES and Pd K-edge XANES/EXAFS spectra reveal that the trivalent palladium ions are stabilized in the $LaPdO_3$ perovskite lattice. The nearly isotropic ($PdO_6$) octahedra in $LaPdO_3$ are probed by Pd K-edge XANES/EXAFS studies, which is consistent with the electronic configuration ($t_{2g}{}^6\sigma^*$) of $Pd^{III}$.

## Acknowledgement

We thank S. Belin and .V. Briois in LURE (French Synchrotron in Orsay) for their help in Pd $L_3$ XAS measurements and the French Ministry of Foreign Affairs for the Pasteur Scholarship of S. J. Kim.

## References

1 N. Bartlett and P. R. Rao, *Proc. Chem. Soc. London*, 1964, 393.
2 F. Langlais, G. Demazeau, J. Portier, A. Tressaud and P. Hagenmuller, *Solid State Commun.*, 1979, **29**, 473.
3 A. Tressaud, S. Khairoun, J. M. Dance, J. Grannec, G. Demazeau and P. Hagenmuller, *C.R. Seances Acad. Sci., Ser. 2*, 1982, **295**, 183.
4 S. Khairoun, J. M. Dance, G. Demazeau and A. Tressaud, *Rev. Chim. Minér.*, 1983, **20**, 871.
5 G. Krämer and M. Jansen, *J. Solid State Chem.*, 1995, **114**, 206.
6 G. Krämer, E. Hägele, N. Wagner and M. Jansen, *J. Solid State Chem.*, 1995, **114**, 206.
7 B.-H. Chen, D. Walker and B. Scott, *Chem. Mater.*, 1997, **9**, 1700.
8 S.-J. Kim, S. Lemaux, G. Demazeau, J.-Y. Kim and J.-H. Choy, *J. Am. Chem. Soc.*, 2001, **123**, 10413.
9 A. W. Sleight, *Mater. Res. Bull.*, 1968, **3**, 699.
10 J. B. Goodenough and J.-S. Zhou, *Chem. Mater.*, 1998, **10**, 2980.
11 J. Rodríguez-Carvajal, FULLPROF, ver. 3.2, LLB-CEA, Saclay, France, 1997.

12 G. Demazeau, I. Omeran, M. Pouchard and P. Hagenmuller, *Mater. Res. Bull.*, 1976, **11**, 1449.
13 F. W. Lytle, G. Van der Laan, R. B. Greegor, E. M. Larson, C. E. Violet and J. Wong, *Phys. Rev. Sect. B*, 1990, **41**, 8995.
14 B. K. Teo, *EXAFS, Basic Principles and Data Analysis*, Springer-Verlag, Berlin, 1986.
15 J.-H. Choy, D.-K. Kim, S.-H. Hwang, G. Demazeau and D.-Y. Jung, *J. Am. Chem. Soc.*, 1995, **117**, 8557.
16 R. D. Shannon, *Acta Crystallogr., Sect. A*, 1976, **32**, 751.
17 J. Rodríguez-Carvajal, M. Hennion, F. Moussa and A. H. Moudden, *Phys. Rev. Sect. B*, 1998, **57**, R3189.
18 J. A. Alonso, M. J. Martínez-Lope, M. T. Casais, J. L. García-Munoz and M. T. Ferández-Diaz, *Phys. Rev. Sect. B*, 2001, **64**, 094102.
19 J. Stöhr, *NEXAFS-spectroscopy*, Springer-Verlag, Heidelberg, 1992.
20 C. de Nadai, A. Demourgues and J. Grannec, *J. Nucl. Instrum. Phys. Res. Sect. B*, 1997, **133**, 1.
21 K. T. Park, D. L. Novikov, V. A. Gubanov and A. J. Freeman, *Phys. Rev. Sect. B*, 1994, **49**, 4425.
22 D. Sondericker, Z. Fu, D. C. Johnston and W. Eberhardt, *Phys. Rev. Sect. B*, 1987, **36**, 3983.
23 M. Medarde, A. Fontaine, J. L. Garcia-Muñoz, J. Rodriguez-Carjaval, M. de Santis, M. Sacchi, G. Rossi and P. Lacorre, *Phys. Rev. Sect. B*, 1992, **46**, 14975.
24 M. Verdaguer, C. Cartier, M. Momenteau, E. Dartyge, A. Fontaine, G. Tourillon and A. Mickalowick, *J. Phys. Colloq.*, 1986, **47**, C8.
25 H. Tolentino, M. Medarde, A. Fontaine, F. Baudelet, E. Dartyge, D. Guay and G. Tourillon, *Phys. Rev. Sect. B*, 1992, **45**, 8091.
26 P. J. Ellis, H. C. Freeman, M. A. Hitchman, D. Reinen and B. Wagner, *Inorg. Chem.*, 1994, **33**, 1248.
27 F. Villain, M. Verdaguer and Y. Dromzee, *J. Phys. IV*, 1997, **7**, C2.
28 J. Etourneau, *Bull. Korean Chem. Soc.*, 1998, **19**, 5.
29 J. H. Choy, J. Y. Kim, S. H. Hwang, S. J. Kim and G. Demazeau, *Int. J. Inorg. Mater.*, 2000, **2**, 61.
30 J. L. García-Munoz, J. Rodríguez-Carvajal and P. Lacorre, *Phys. Rev. Sect. B*, 1994, **50**, 978.